AD-A154 508 CAPACITIVE ENERGY STORAGE AT CRYOGENIC TEMPERATURES(U) 1/1
CERAMPHYSICS INC WESTERVILLE OH W N LAWLESS ET AL.
15 FEB 85 AFOSR-TR-85-0377 F49620-84-C-0089
UNCLASSIFIED F/G 10/2 NL

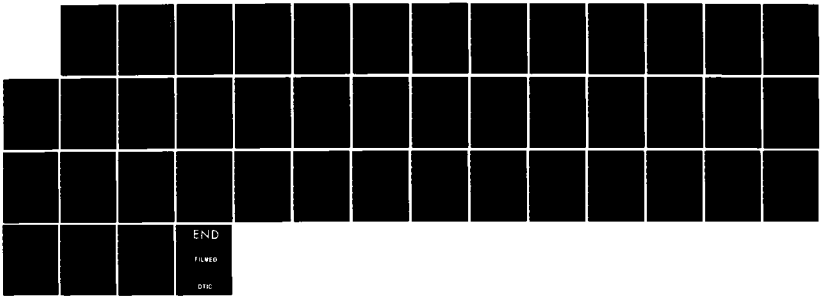

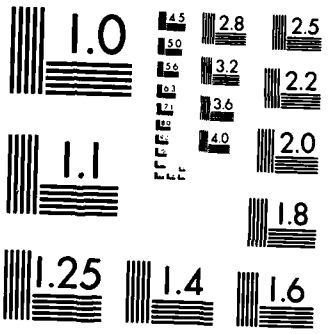

Unclassified
SECURITY CLASSIFICATION OF THIS PAGE

(2)

REPORT DOCUMENTATION PAGE

1a. REPORT SECURITY CLASSIFICATION: Unclassified	1b. RESTRICTIVE MARKINGS: None
AD-A154 508 EDULE	3. DISTRIBUTION/AVAILABILITY OF REPORT: Approved for public release; distribution unlimited. Unrestricted
IMBER(S)	5. MONITORING ORGANIZATION REPORT NUMBER(S): AFOSR-TR- 85-0377
6a. NAME OF PERFORMING ORGANIZATION: CeramPhysics, Inc. / 6b. OFFICE SYMBOL (If applicable):	7a. NAME OF MONITORING ORGANIZATION: AFOSR
6c. ADDRESS (City, State and ZIP Code): 921 Eastwind Drive, Suite 110, Westerville, Ohio 43081	7b. ADDRESS (City, State and ZIP Code): Bolling AFB, Washington, D.C. 20332
8a. NAME OF FUNDING/SPONSORING ORGANIZATION: AFOSR / 8b. OFFICE SYMBOL (If applicable): NP	9. PROCUREMENT INSTRUMENT IDENTIFICA: Contract #F49620-84-C-0089
8c. ADDRESS (City, State and ZIP Code): Bolling AFB, Washington, D.C. 20332	10. SOURCE OF FUNDING NOS.

PROGRAM ELEMENT NO.	PROJECT NO.	TASK NO.	WORK UNIT NO.
61102F	3005	A1	

11. TITLE (Include Security Classification): Capacitive Energy Storage at Cryogenic Temperatures

12. PERSONAL AUTHOR(S): W.N. Lawless, C.F. Clark

13a. TYPE OF REPORT	13b. TIME COVERED	14. DATE OF REPORT (Yr., Mo., Day)	15. PAGE COUNT
Final	FROM 9/1/84 TO 2/28/85	1985 February 15	40

16. SUPPLEMENTARY NOTATION: None

17. COSATI CODES			18. SUBJECT TERMS (Continue on reverse if necessary and identify by block number)
FIELD	GROUP	SUB. GR.	Energy Storage Prime Power Systems

19. ABSTRACT (Continue on reverse if necessary and identify by block number)

A Phase I research program on capacitive energy storage at liquid-nitrogen temperatures is reported. A composition in the cadmium-lead-niobate-tantalate family of ceramic ferroelectrics was chosen with a paraelectric→ferroelectric phase transition at 71 K (so-called CPN17 composition), and prototype multilayer capacitors (MLC's), 1 X 1 X 0.2 cm^3 with 46 active layers, were fabricated for testing. Dielectric constant, specific heat, and electrocaloric data were measured on these MLC's in the range 77 - 100 K at electric fields up to 200 kV/cm.

All the measured data can be explained and correlated very satisfactorily using a Ginzburg-Landau expansion of the free energy in combination with the TdS equation for dielectrics.

Capacitive-energy-storage densities were computed from the measured electric-field dependence of the dielectric constant at 77 K using the Helmholtz integral. A state-

20. DISTRIBUTION/AVAILABILITY OF ABSTRACT	21. ABSTRACT SECURITY CLASSIFICATION
UNCLASSIFIED/UNLIMITED ☒ SAME AS RPT. ☐ DTIC USERS ☐	UNCLASSIFIED

22a. NAME OF RESPONSIBLE INDIVIDUAL	22b. TELEPHONE NUMBER (Include Area Code)	22c. OFFICE SYMBOL
Maj. Pugh	(202) 767-4908	NP

DD FORM 1473, 83 APR EDITION OF 1 JAN 73 IS OBSOLETE.

Unclassified
SECURITY CLASSIFICATION OF THIS PAGE

85 4 23 177

switching phenomenon was observed: Above ~300 kV/cm, CPN17 switches to a new, highly polarizable state, and the Helmholtz energy density for this state is ~55 J/cm^3 ≅ 9 J/g (measured to 1.08 MV/cm). This induced state is non-hysteretic. In the absence of state-switching, the energy density is 1 - 2 J/g (i.e., obtained by extrapolating the dielectric data measured up to ~200 kV/cm).

The zero-field specific heat of CPN17 is 0.15 J g^{-1} K^{-1} at 77 K and displays an excess specific heat centered around 82 K. The "background" specific heat of CPN17 is characterized by an effective Debye temperature of 442 K, and the effect of an electric field is to suppress the specific heat but this effect is not large (~6% at 200 kV/cm).

Reversible, electrocaloric effects are demonstrated in CPN17 at 77.7 and 94.3 K, and these temperature changes are ~0.8 K at 130 kV/cm. Thus, electrocaloric cooling by adiabatic depolarization on discharge (E → 0) is available in CPN17 as possible stabilization mechanism to compensate irreversible heating effects, and the energy density available is ~1 J cm^{-3}.

Joule heating in the thin metal electrodes of the MLC on charge/discharge is examined. It is concluded that this heating effect is minor even under extreme conditions--i.e., the associated temperature rise in the adjacent ceramic is ~2mK.

The technical goals of this Phase I study have been met (exceeded, actually), and areas of further research in a Phase II program are recommended.

FINAL REPORT

on

Capacitive Energy Storage at Cryogenic Temperatures

Phase I, AFOSR-SBIR

Contract F49620-84-C-0089

by

W.N. Lawless and C.F. Clark

CeramPhysics, Inc.

P.O. Box 346

Westerville, Ohio 43081

February 15, 1985

Distribution

H.L. Pugh, Jr., Bolling AFB (6 Copies)
C.E. Oberly, WPAFB (1 Copy)
N. Harold, WPAFB (1 Copy)

I. SUMMARY

A Phase I research program on capacitive energy storage at liquid-nitrogen temperatures is reported. A composition in the cadmium-lead-niobate-tantalate family of ceramic ferroelectrics was chosen with a paraelectric ⇄ ferroelectric phase transition at 71 K (so-called CPN17 composition), and prototype multilayer capacitors (MLC's), 1 x 1 x 0.2 cm^3 with 46 active layers, were fabricated for testing. Dielectric-constant, specific-heat, and electrocaloric data were measured on these MLC's in the range 77 - 100 K at electric fields up to 200 kV/cm.

All the measured data can be explained and correlated very satisfactorily using a Ginzburg-Landau expansion of the free energy in combination with the TdS equation for dielectrics.

Capacitive-energy-storage densities were computed from the measured electric-field dependence of the dielectric constant at 77 K using the Helmholtz integral. A state-switching phenomenon was observed. Above ~ 300 kV/cm, CPN17 switches to a new, highly polarizable state, and the Helmholtz energy density for this state is ~ 55 J/cm^3 ≈ 9 J/g (measured to 1.08 MV/cm). This induced state is non-hysteretic. In the absence of state-switching, the energy density is 1 - 2 J/g (i.e., obtained by extrapolating the dielectric data measured up to ~ 200 kV/cm).

The zero-field specific heat of CPN17 is 0.15 $J/g^{-1}/K^{-1}$ at 77 K and displays an excess specific heat centered around 82 K. The "background" specific heat of CPN17 is characterized by an effective Debye temperature of 442 K, and the effect of an electric field is to suppress the specific heat but this effect is not large (~ 6% at 200 kV/cm).

Reversible, electrocaloric effects are demonstrated in CPN17 at 77.7 and 94.3 K, and these temperature changes are ~ 0.8 K at 130 kV/cm. Thus, electrocaloric cooling by adiabatic depolarization on discharge ($E \rightarrow 0$) is available in CPN17 as a possible stabilization mechanism to compensate irreversible heating effects, and the energy density available is ~ 1 J cm^{-3}.

Joule heating in the thin metal electrodes of the MLC on charge/discharge is examined. It is concluded that this heating effect is minor even under extreme conditions --i.e., the associated temperature rise in the adjacent ceramic is ~ 2mK.

The technical goals of this Phase I study have been met (exceeded, actually), and areas of further research in a Phase II program are recommended.

II. INTRODUCTION

Storing energy in capacitor banks at room temperature is commonly used in applications where size or weight has not been a major concern. However, capacitive-energy-storage at cryogenic temperatures offers considerable advantages: (1) Dielectric breakdown strengths in ceramic capacitors are enhanced; (2) Deleterious effects due to electronic conduction and/or aging in ferroelectric ceramics may be frozen out; (3) Electrical resistivities of metal components are decreased by an order of magnitude compared to room temperature; and (4) A judicious choice of ceramic compositions can lead to electrocaloric cooling effects on discharge ($E \rightarrow 0$) which can partially offset irreversible heating effects. Finally, both liquid nitrogen (77.4 K) and liquid oxygen (90.2 K) are

inexpensive cryogens with large latent heats, and the latter cryogen is available on spacecraft.

There are few published studies of capacitive energy storage at cryogenic temperatures. A General Electric study[1] in the late 60's reported energy densities ≈ 0.6 J/cm^3 at 77 K, and a Corning Glass Works study[2] reported densities up to ~ 5 J/cm^3 at 77 K.

From basic research at CeramPhysics in the cadmium-lead-niobate-tantalate family of ferroelectric ceramics, a composition range was discovered which has a very large maximum in the dielectric constant (≈ 7000) at liquid-nitrogen temperatures, and the paraelectric → ferroelectric transition temperature can be compositionally varied from 50 to 150 K. Early estimates of the energy density values possible with these ceramics at cryogenic temperatures suggested 20 - 25 J/cm^3, and these materials sinter in a temperature range favorable for making multilayer capacitors (MLC's) using state-of-the-art, tape-casting manufacturing methods.

These concepts led to the funding of this Phase I research program to explore the dielectric and thermal properties of a ceramic composition with a transition temperature ≈ 70 K. This Final Report is organized along the following lines: First, in Section III the theoretical concepts will be reviewed, as this will set the venue of the report and explain why certain measurements were made from a thermodynamic point of view. Section IV will describe the experimental methods used, and in Section V the E-field dependent dielectric measurements will be presented which bear directly on capacitive energy storage. The results of specific heat and electrocaloric measurements will be presented in Section VI, and a complete thermodynamic analysis of all the dielectric

and thermal data along the theoretical lines of Section III will be given in Section VII. The report will conclude with Sections VIII (Discussion and Conclusions) and IX (Recommendations for Future Studies).

For easy reference the symbols used in the text are summarized below:

E	Electric field strength
P	Polarization
ϵ_E	Dielectric constant at E
ΔF	Helmholtz energy density
C_E	Specific heat at E
ρ	Density
ΔT_e	Reversible electrocaloric temperature changes
χ, ζ, ξ	Ginzburg-Landau expansion coefficients

III. THEORETICAL CONSIDERATIONS

In this section, the theoretical concepts needed to understand the physics of capacitive energy storage and the associated electrocaloric effects will be reviewed, and this section will also provide a background for the experiments undertaken.

The dielectric state variables are P,E, and T, and for ferroelectrics these are related through the Ginzburg-Landau expansion of the Gibbs free energy,[3]

$$A = A_0 + \frac{1}{2}\chi_0 P^2 + \frac{1}{4}\xi P^4 + \frac{1}{6}\zeta P^6 + \ldots \quad (1)$$

which has the definitional properties that

$$E = \partial A/\partial P = \chi_0 P + \xi P^3 + \zeta P^5 + \ldots \quad (2)$$

and

$$\chi_E = 4\pi/\varepsilon_E = \partial E/\partial P = \chi_0 + 3\xi P^2 + 5\zeta P^4 + \ldots \quad (3)$$

Here χ is the dielectric susceptibility, and Eq. (1) has the symmetry of a cubic paraelectric material such as the pyrochlore ceramics in this program. It is usual to assume that only the χ_0 coefficient is temperature dependent, $\chi_0 \propto T-T_0$ (the Curie-Weiss law). We remark, however, that all three phase transitions in $BaTiO_3$ have been accounted for within this formalism by allowing ξ and ζ to have a small temperature dependence also.[4]

The energy available in an isothermal process for reversible conditions is the Helmholtz density

$$\Delta F = \int E dP \quad (4)$$

which from Eq. (3) becomes

$$\Delta F = \frac{1}{8\pi} \int_0^{E_c^2} \varepsilon_E dE^2. \quad (5)$$

Equation (5) is one of the central results of this section and illustrates that capacitive energy-storage densities are directly found from the E-field dependence of the dielectric constant. The field E_c in Eq. (5) is an upper field limit, and ΔF depends quadratically on E_c, underscoring the desirability of the large breakdown strengths that may be achievable in ceramic capacitors at cryogenic temperatures.

The expansion Eq. (1) is in powers of P for ferroelectrics because the spontaneously polarized state is defined as $P \neq 0$ for $E = 0$, and Eq. (2) yields properties of the coefficients (e.g., for a second-order transition, $\xi > 0$). For our purposes, it is more convenient to invert Eq. (2), and substituting in Eq. (3) we have

$$\chi_E = \chi_0 + (3\xi/\chi_0^2)E^2 + (5\zeta/\chi_0^4 - 6\xi^2/\chi_0^5)E^4 + \ldots \quad (6)$$

for the explicit E-field dependence of $\varepsilon_E = 4\pi/\chi_E$.

Turning next to the thermal properties, the reversible electrocaloric properties are described by the TdS equation for dielectrics[5]

$$TdS = C_E dT + T(\partial P/\partial T)_E dE \quad (7)$$

which for the adiabatic processes ($dS = 0$) leads to the differential equation

$$C_E dT/T = -(\partial P/\partial T)_E dE \quad (8)$$

We now assume that in the low-field region the relative temperature changes dT/T are small and the E-field dependence of the specific heat is small also. Therefore, inverting Eq. (2), performing the derivative $\partial P/\partial T$, and performing the integration in Eq. (8) we have

$$C_E \Delta T_e/T \cong aE^2 + bE^4 + cE^6 + \ldots \tag{9}$$

where

$$\begin{aligned} a &= \dot{\chi}_0/2\chi_0^2 \\ b &= -\xi\dot{\chi}_0/\chi_0^5 \\ c &= \dot{\chi}_0(21\xi^2/6\chi_0^8 - \zeta/\chi_0^7) \end{aligned} \tag{10}$$

where $\dot{\chi}_0 = d\chi_0/dT = -(4\pi/\varepsilon_0^2)d\varepsilon_0/dT$, and the temperature dependences of ξ and ζ have been ignored.

Equation (9) is the simplest theromodynamic expression relating the specific heat and electrocaloric data to the dielectric data through the Ginzburg-Landau coefficients, and we shall use Eqs. (6), (9) and (10) in Section VIII to correlated all these data.

Equations (8) and (9) reveal an important finding. Namely, on general grounds $\partial P/\partial T \propto d\varepsilon_0/dT$ (note that the T-dependence of ζ and ξ is generally very small compared to that of χ_0). Consequently, the electrocaloric cooling effects on discharge will scale with $d\varepsilon_0/dT$, and this is an important practical result for maximizing (or minimizing) electrocaloric effects.

Finally, we address the problem of Joule heating in the thin metal electrodes of a multilayer ceramic capacitor on charge/discharge, as these electrodes could represent the largest resistance component in the

energy-storage circuit. We construct the following simple model: Consider a single, electroded ceramic layer of thickness d, length ℓ, and width w. The metal electrode has a thickness δ so that the electrode resistance is

$$R_e = (\rho_e/\delta)(\ell/w) \tag{11}$$

where ρ_e is the electrode resistivity.

The total energy stored in this single-layer capacitor is

$$Q\Delta V \cong v\Delta F \tag{12}$$

where v is the ceramic volume ($\ell\omega d$), Q is the charge, V is the voltage, and ΔF is given by Eq. (5). The Joule heat generated in the electrode is

$$u = i^2 R_e \Delta t \tag{13}$$

where i is the current carried by the electrode and Δt is the charge/discharge time. Approximating $i \simeq Q/\Delta t$ and combining with Eq. (11), Eq. (13) becomes

$$u \simeq Q^2(\rho_e/\delta)(\ell/\omega)/\Delta t \tag{14}$$

The charging field is $E_c = \Delta V/d$, and combining Eqs. (12) and (14) we have the final result

$$u \simeq (\rho_e/\delta)(w\ell^3/\Delta t)(\Delta F/E_c)^2 \qquad (15)$$

Equation (15) reveals several practical features. For example, the factor $\omega\ell^3/\Delta t$ will be large for large capacitors and fast discharge times, but u is independent of the ceramic thickness. Also, since $\Delta F \propto E_c^2$ from Eq. (5), Eq. (15) indicates that $u \propto E_c^2$. Numerical examples based on Eq. (15) will be given in Section VIII.

IV. EXPERIMENTAL METHODS

Sample Preparation

Based on CeramPhysics' research at cryogenic temperatures in the cadmium-lead-niobate-tantalate family of ferroelectric ceramics, a composition was selected which had a paraelectric-ferroelectric transition temperature ≃ 70 K, thus insuring a cubic pyrochlore material at 77 K. This composition is labelled CPN17 in what follows, and prototype multilayer capacitors (MLC's) were fabricated from this composition.

In designing the multilayer capacitors for testing, the two most important considerations were the size of the MLC and the dielectric thickness. That is, the MLC could not exceed about 1 x 1 x 0.5 cm^3 due to space limitations in the adiabatic calorimeter, and it was desirable to have the dielectric thickness be as small as possible to achieve large electric-field strengths. After some testing with cast ceramic tapes of CPN17, it was decided to design the MLC's with fired dimensions 1 x 1 x 0.2 cm^3 wherein there were 46 active dielectric layers with electroded areas about 0.8 x 0.8 cm^2 per layer. The dielectric thickness was designed to be less than 50 μm (.002") after firing.

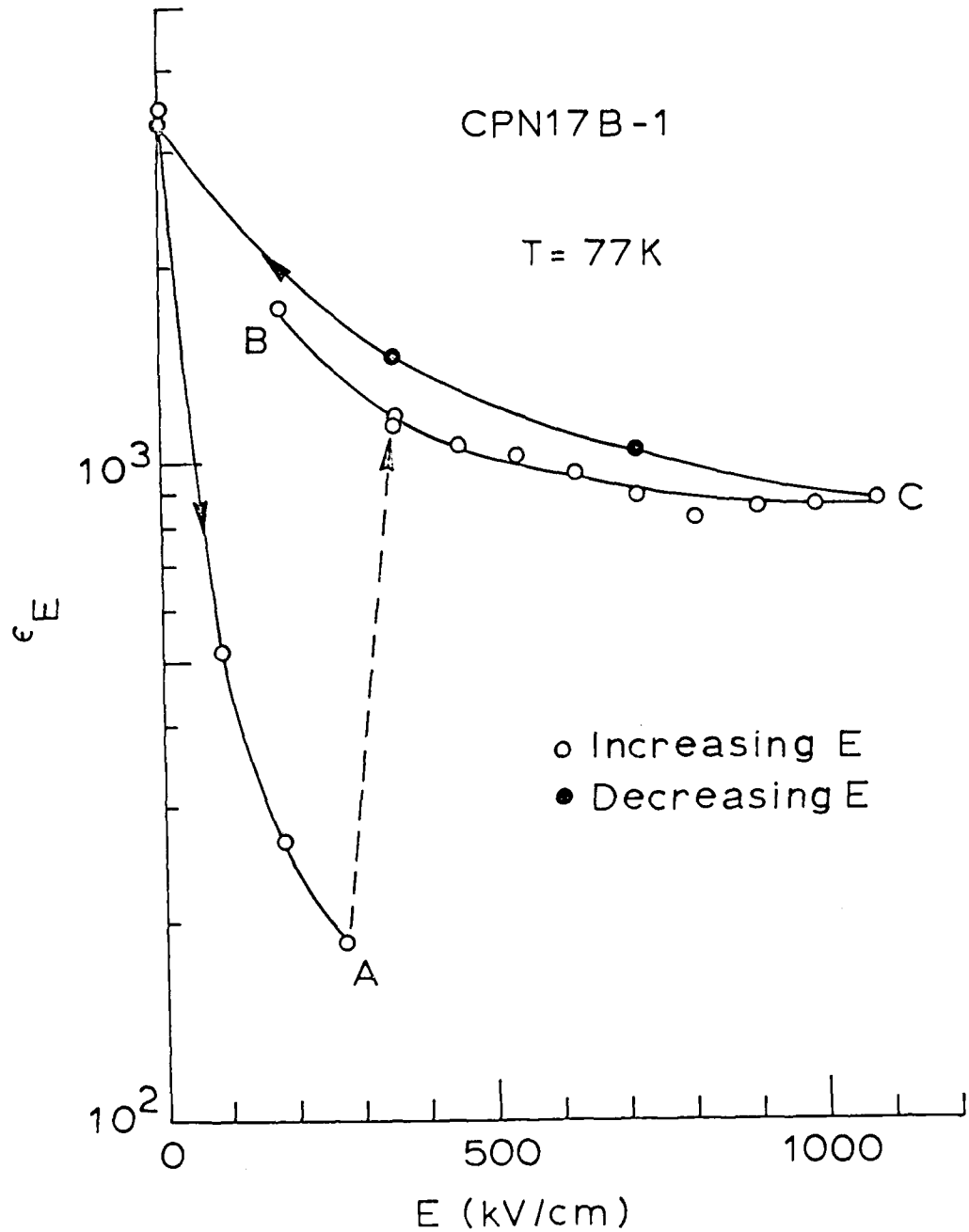

Figure 6. Electric-field dependence of the dielectric constant of CPN17B-1 at large field strengths. Switching to a stable, non-hysteretic state above ~ 300 kV/cm is indicated.

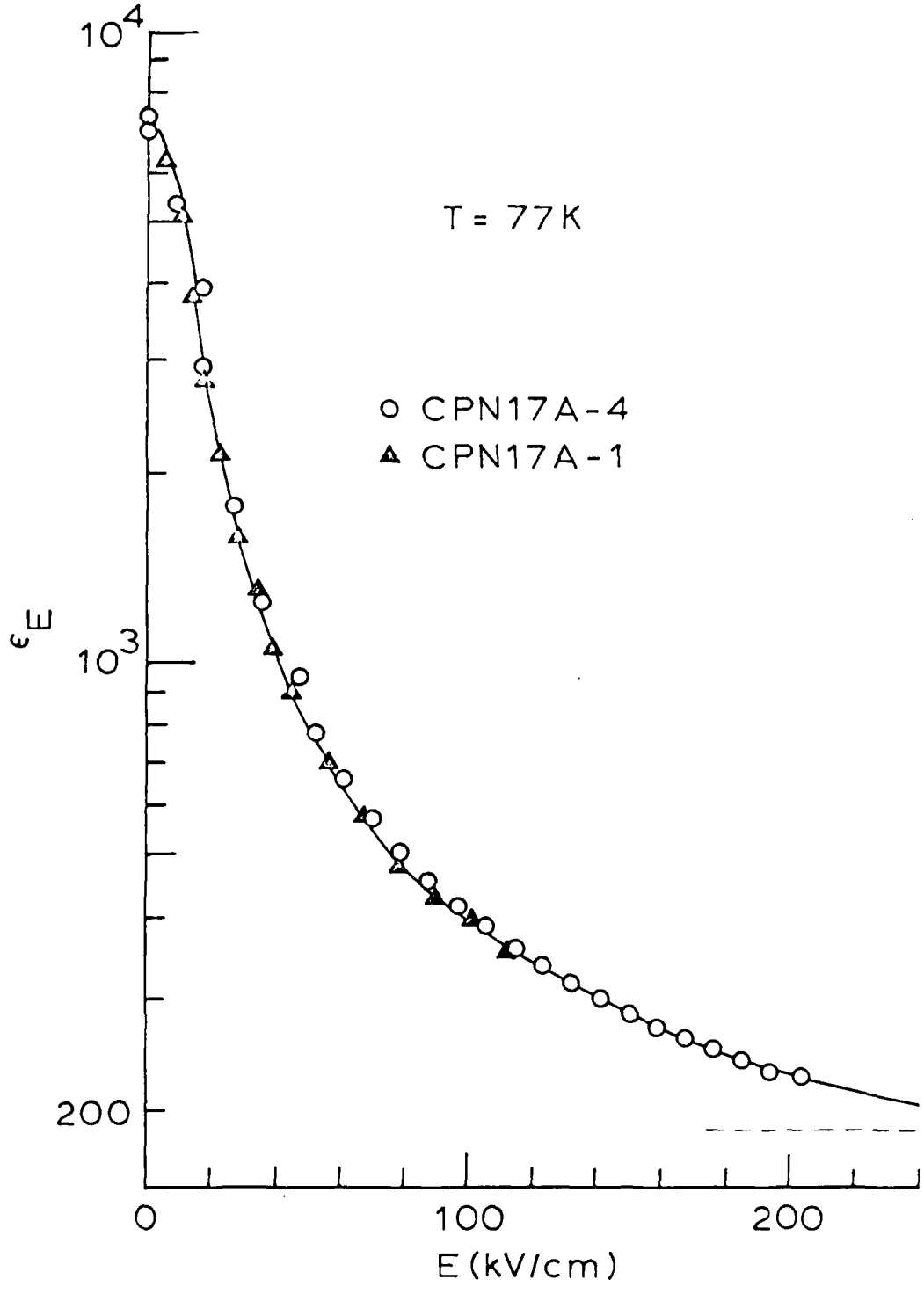

Figure 5. Field-dependent dielectric data at 77 K measured on two MLC's showing the unit-to-unit reproducibility of the data.

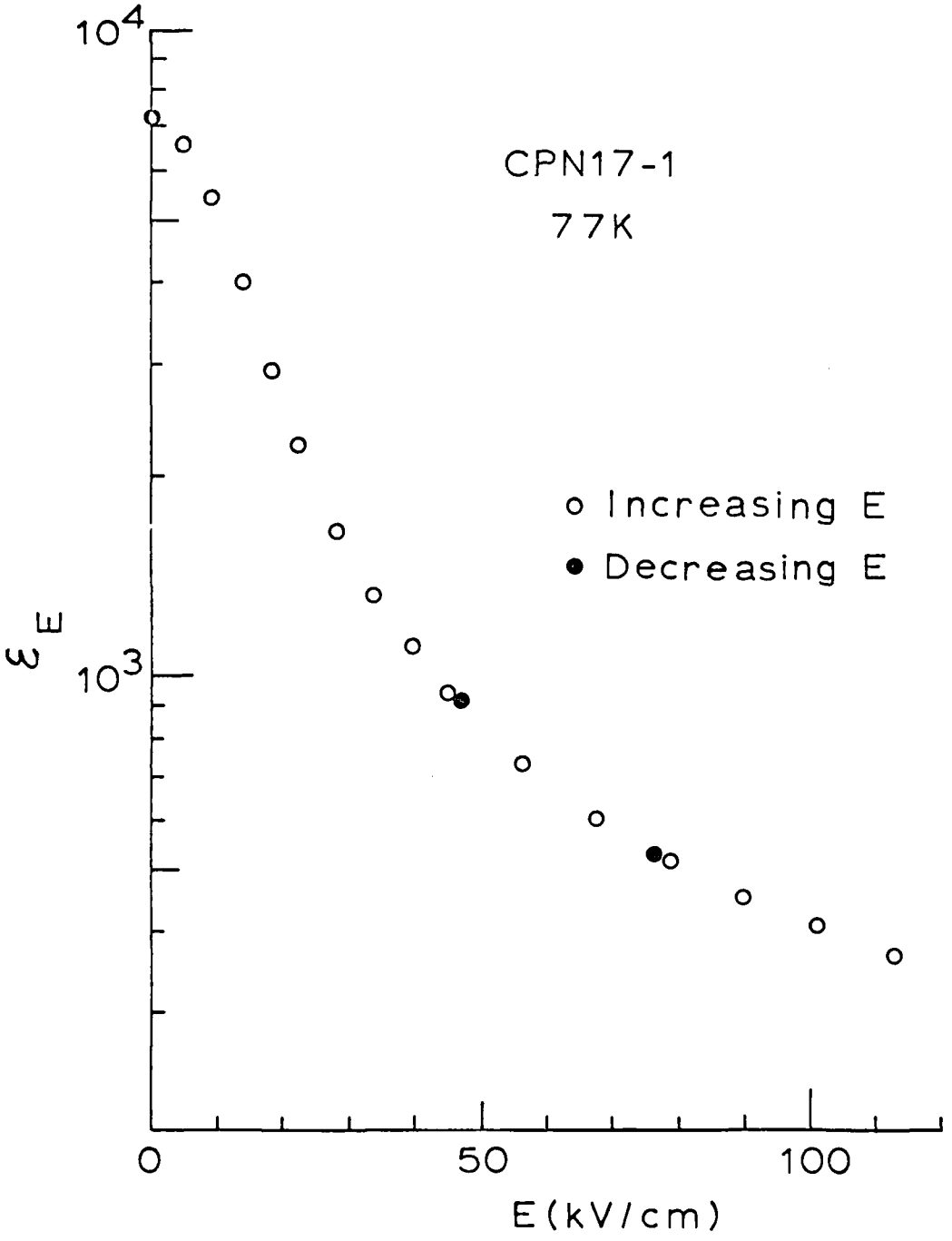

Figure 4. Field-dependent dielectric data at 77 K measured on one of the CPN17 MLC's. These and other measurements showed the absence of any hysteretic effects in CPN17.

show that the CPN17 ceramic in the MLC has the desired properties (ε_{max} ~ 7000 at ~ 70 K) and that $d\varepsilon_0/dT$ is quite large, ~ 100 K^{-1} at ~ 90 K).

Field-dependent dielectric data, ε_E, at 77 K are shown in Fig. 4, and these data reveal a property of CPN17 that was universally found at or above 77 K; namely, the ε_E-curve is exactly reproducible on increasing and decreasing E, indicating the complete absence of hysteretic effects. This is an important practical result for capacitive energy storage.

Field dependent ε_E-data measured on two MLC's are shown in Fig. 5, and an excellent unit-to-unit reproducibility is seen. The ε_E-data appear to saturate, and a graphical extension of the data indicates $\varepsilon_\infty \simeq 195$ as indicated by the dashed line in Fig. 5 (See below).

One of the MLC's from the second-batch of MLC's withstood 3000 V in the course of ε_E measurements at 77 K, and these data are shown in Fig. 6. A very interesting effect is seen: Up to point A, ε_E drops rapidly with E, but at E ≃ 300 kV/cm ε_E switches onto the curve B-C and is apparently stable as E is varied along the B-C curve. On decreasing E from point C to zero, the original value of ε_0 is reproduced very well. This value of ε_0 (~ 3500) differs from ε_0 in Fig. 5 (~ 7000), and this may be due to the finer particle-size ceramic used in the second batch of MLC's.

Several attempts were made to reproduce the data in Fig. 6, and although the curve up to point A could be reproduced very well with the second-batch MLC's, no MLC could withstand E ≃ 300 kV/cm (including the original MLC of Fig. 6 which failed on re-measuring).

It was wondered if the electronic system (i.e., bridge + extension components + protection circuitry) were acting anomalously at large

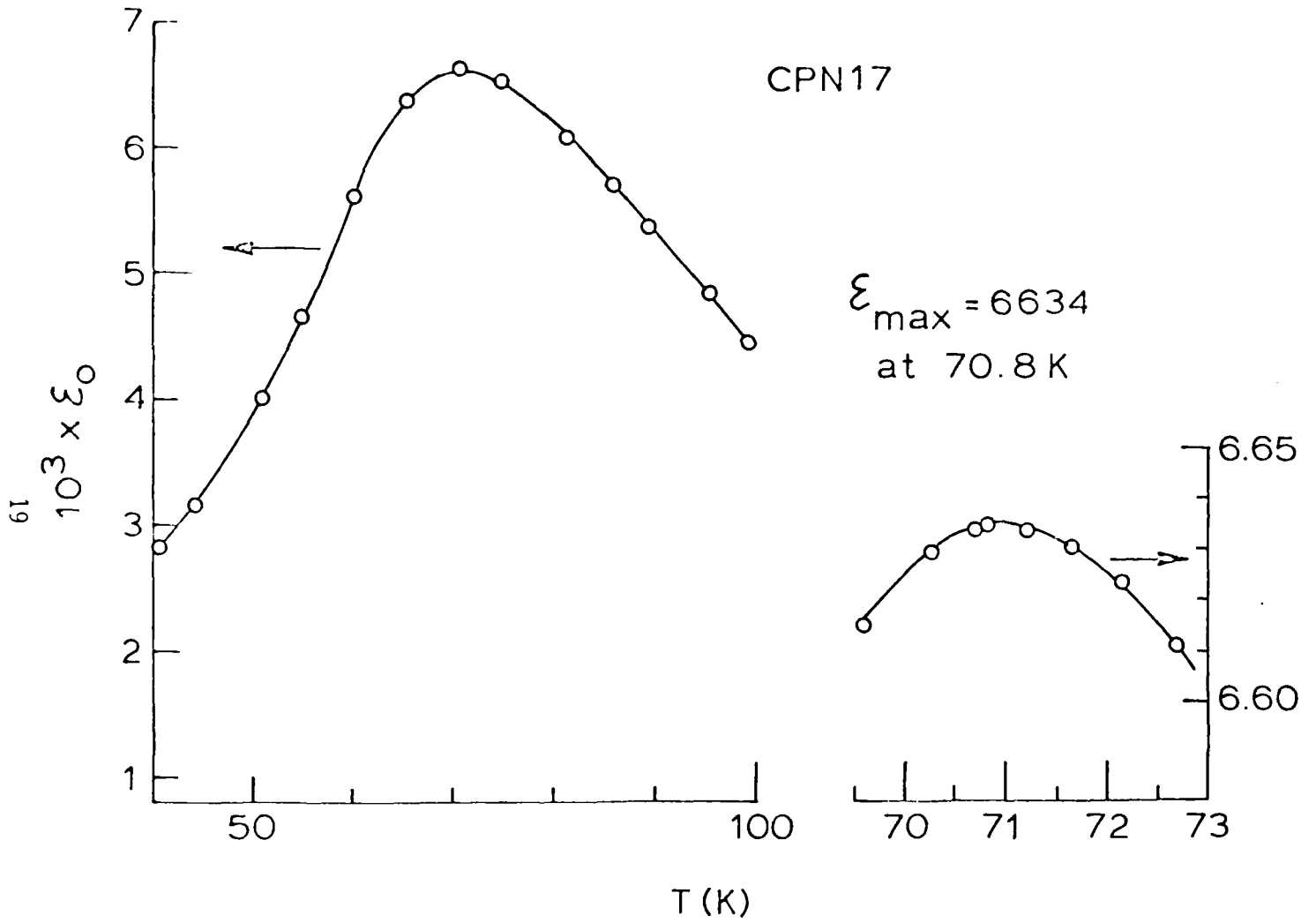

Figure 3. Zero-field dielectric data measured as a function of temperature on an MLC of CPN17.

applying Eq. (18) that the inactive ceramic is included in the addenda and that C_s is the heat capacity at that E-field level.

Finally, in the field cycle $0 \rightarrow E \rightarrow 0$ there may be an asymmetry in the polarization and depolarization temperature changes, and this is a sensitive test for hysteretic (irreversible) effects. These can be separated by writing each ΔT as the sum of reversible and irreversible parts, where the former depends on the sign of ΔE but the latter does not.[10] The reversible part is called ΔT_e in this report.

Electrode Resistance Measurements

One of the CPN17 MLC's was cut on a diamond saw to expose all the Pt/Pd/Au electrodes on the two termination faces, and the resistance between these two faces was measured using four-lead dc potentiometric methods. Several current levels between 1 - 10 mA were used, and the current was reversed to eliminate thermal emf's. The MLC had 47 electrodes constituting 47 parallel resistors in this sample, and the resistance per electrode was 0.145 Ω at 300 K, 2.90 Ω at 77 K. Each electrode was 0.74 cm long in the current direction and 0.80 cm wide, so that the quantity $\rho_e \delta$ entering Eq. (15) is 3.14 Ω at 77 K. The electrodes were found to be ohmic at both temperatures.

V. DIELECTRIC RESULTS

The theoretical discussion in Section III indicates the need for $\varepsilon_0(T)$ data -- ε_0 enters the leading term in Eq. (3), $d\varepsilon_0/dT$, the leading term in Eq. (9). These measured data are shown in Fig. 3, 40 - 100 K, and the inset data show detail around the peak at 70.8 K. These data

three Keithley Model 181 nanovoltmeters IEEE-interfaced with a DEC 350 computer programmed to read the nanovoltmeters every 20 sec [dt in Eq. (17)]. The $T\text{-}T_r\text{-}\Delta t$ data record generated is then analyzed according to Eq. (17) to give the desired $C_E(T)$ data.

There is a subtlety involved in reducing these C_E data; namely, only ~ 60% of the CPN17 ceramic in the MLC is exposed to the E-field due to the pullback and cover plates (larger MLC's would be much more dielectrically efficient). Therefore, this "inactive volume" of the ceramic is treated as an addendum, and the pulse, C_o-data are used to make this correction.

The electrocaloric data are measured in a straightforward fashion: After stabilizing the reservoir at some desired temperature, the MLC temperature changes are measured on cycling the field $0 \rightarrow E_1 \rightarrow 0$, $0 \rightarrow E_2 \rightarrow 0$, etc. The temperature rises on adiabatic polarization ($0 \rightarrow E$) and on adiabatic depolarization ($E \rightarrow 0$) are determined by measuring the thermometer-voltage changes on a Hewlett Packard Model 7128A chart recorder. A high voltage switch box was constructed for rapidly switching the voltage on and off the sample because the time constant of the power supply for $V \rightarrow 0$ was too long.

The actual and measured temperature changes are related by

$$\Delta T_{actual} = \Delta T_{meas} \quad (1 + C_a/C_s), \tag{18}$$

where C_a is the heat capacity of the addenda and C_s is the heat capacity of the ceramic exposed to the E-field, and Eq. (18) reflects the fact that the "active" ceramic is thermally loaded by the addenda. Note in

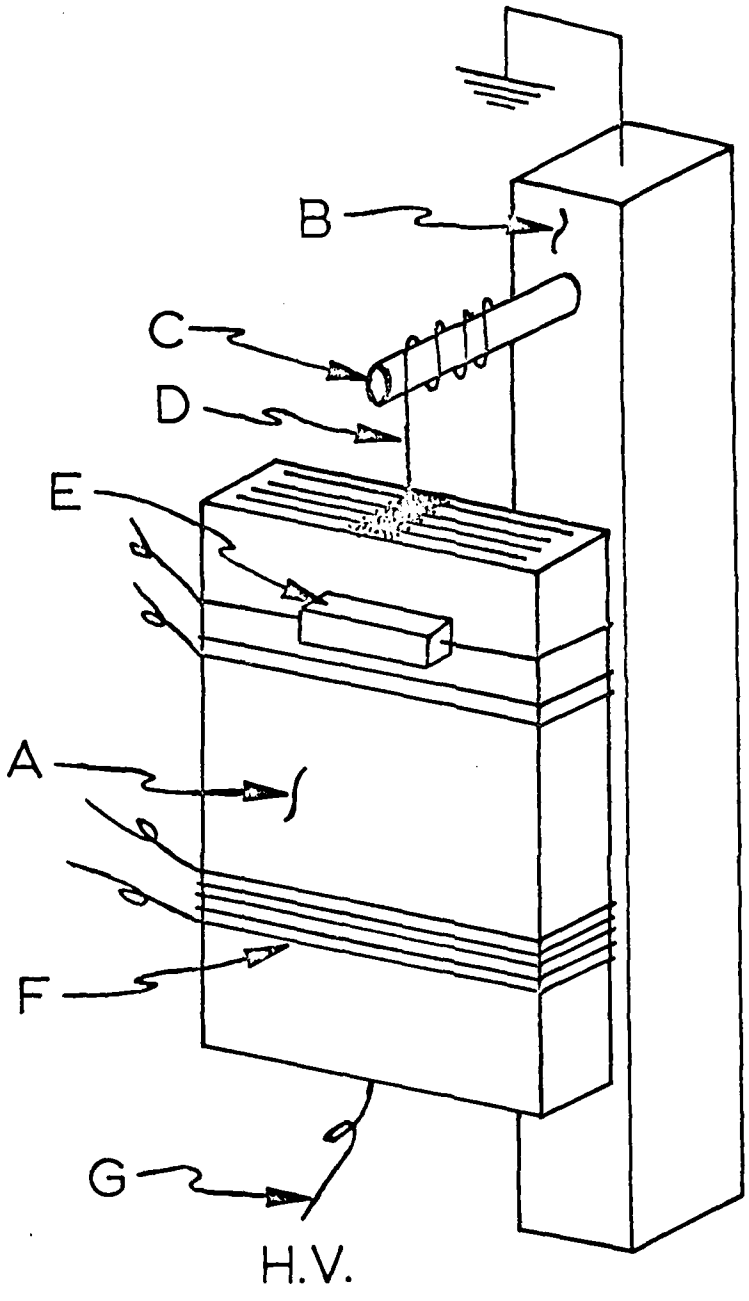

Figure 2. Schematic drawing of the MLC mounting for specific heat and electrocaloric measurements. The MLC (A) is fixtured with a thermometer (E) and heater (F) and suspended on a thermal link (D) from a copper post (C) bolted into the reservoir (B) at ground potential. A high voltage lead (G) is attached to the opposite side of the MLC with silver paste.

metal electrodes in the MLC (40 Pt, 20 Pd, 40 Au) constitute an addendum but could not be determined independently. From the measured densities of the MLC's, an average electrode weight was determined, 25.1 mg per MLC.

The first step in these thermal measurements was to measure the zero-field specific heat, C_0, by the standard, dynamic-pulse method.[6] The E-field dependence of the specific heat was measured by a drift method. Referring to Fig. 2, with the reservoir stabilized at 77 K, the heater was used to bring the MLC to some elevated temperature ($\sim$ 95 K). Then, after de-activating the heater, the MLC temperature slowly drifted in time to the reservoir temperature according to

$$C_t(dT/dt) = - \int_{T_r}^{T} G dT \qquad (17)$$

where C_t is the total heat capacity, T_r is the reservoir temperature, and G is the thermal conductance of the link (D in Fig. 2). The advantage of this method is that several drifts can be made at various E-fields using automated data-collection methods once the conductance of the link is calibrated.

The link is calibrated from a drift at E = 0 as follows: The pulse heat capacity data are combined with the measured (dT/dt) data in the l.h.s. of Eq. (17), and G(T) is expanded in powers of T for integrating the r.h.s. of Eq. (17). Regression analyses are then used to determine the expansion coefficients which then calibrate the link.

The method is implemented as follows: The carbon thermometer on the MLC and the Pt thermometer are wired in series, and the common exciting current and the two thermometer voltages are measured using

bridge. Two types of measurements were made: (1) ϵ_0 vs. T, 40 - 100 K; and (2) ϵ_E vs. E at 77 K. The former measurement was made in a temperature-controlled, two-can cryostat, and the latter measurements were made by immersing the MLC directly in a dewar of liquid nitrogen.

Dielectric breakdown measurements at cryogenic temperatures were made inadvertently in the course of other measurements.

Specific Heat and Electrocaloric Measurements

Equations (7) - (9) above show the intimate relation between the specific heat and the electrocaloric properties, and all of these measurements were made in a temperature-controlled, two-can, adiabatic calorimeter.[6] The MLC's measured were mounted in the calorimeter as shown in Fig. 2. The MLC (A) was fixtured with a heater (F, ~ 300 Ω), carbon-chip thermometer (E, ~ 10 mg), and thermal link (D) using G.E. 7031 varnish, and the weights of these addenda were determined by cumulative weighings. A thin manganin lead (G) connected half of the MLC electrodes to the high-voltage supply, and the other half of the electrodes were connected to ground by the thermal link (D) which was indium-soldered to a copper pin (C) bolted into the reservoir (B).

A calibrated Pt thermometer was mounted in the reservoir (B), and the carbon thermometer (E) was ground from a 470 Ω, 1/8 W, Allen-Bradley resistor and calibrated in the course of the run according to[7]

$$\log R = A + BT^{-P}. \tag{16}$$

The addenda corrections in the liquid-nitrogen range (i.e., for manganin, silver, 7031, etc.) were made using literature data.[8,9] The

voltage is applied to the circuit. As the blocking capacitor and sample are charged through the isolation resistors, no voltage will appear across the bridge terminals. After a time period greater than several time constants, the shorting switch is opened and the capacitance reading is taken on the bridge. The isolation resistors (2.7 MΩ) prevent the bridge from "seeing" the high voltage supply.

The calculation of the sample capacitance takes into account the series blocking capacitor (nominal 3 μf from Maxwell Laboratories) and the parallel (small) capacitances of the neon light, etc. For small sample capacitances the blocking capacitor may be treated as an infinite capacitance in the first approximation. If the sample is larger, or if more accuracy is required, the exact value of the blocking capacitance and the dependence of this value on voltage needs to be known. These values were measured with the help of an additional, identical capacitor supplied by Maxwell Laboratories.

In case of problems (e.g., sample breakdown) there are several protective devices built into the circuit to protect the bridge. Large current flows are prevented by the fuse (AGX 2) in series with the blocking capacitor. Two redundant systems protect the bridge from voltages appearing across the input leads. There is a pair of zener diodes between each input lead and the capacitor case (equivalent to the lead shields). These are large wattage zeners and are selected to trigger at a low voltage (14 V in this case). The redundant neon lamp will also become conductive once the voltage across it reaches a threshold value.

All capacitance measurements in this program were made by the three-terminal method using coaxial cables from the sample to the

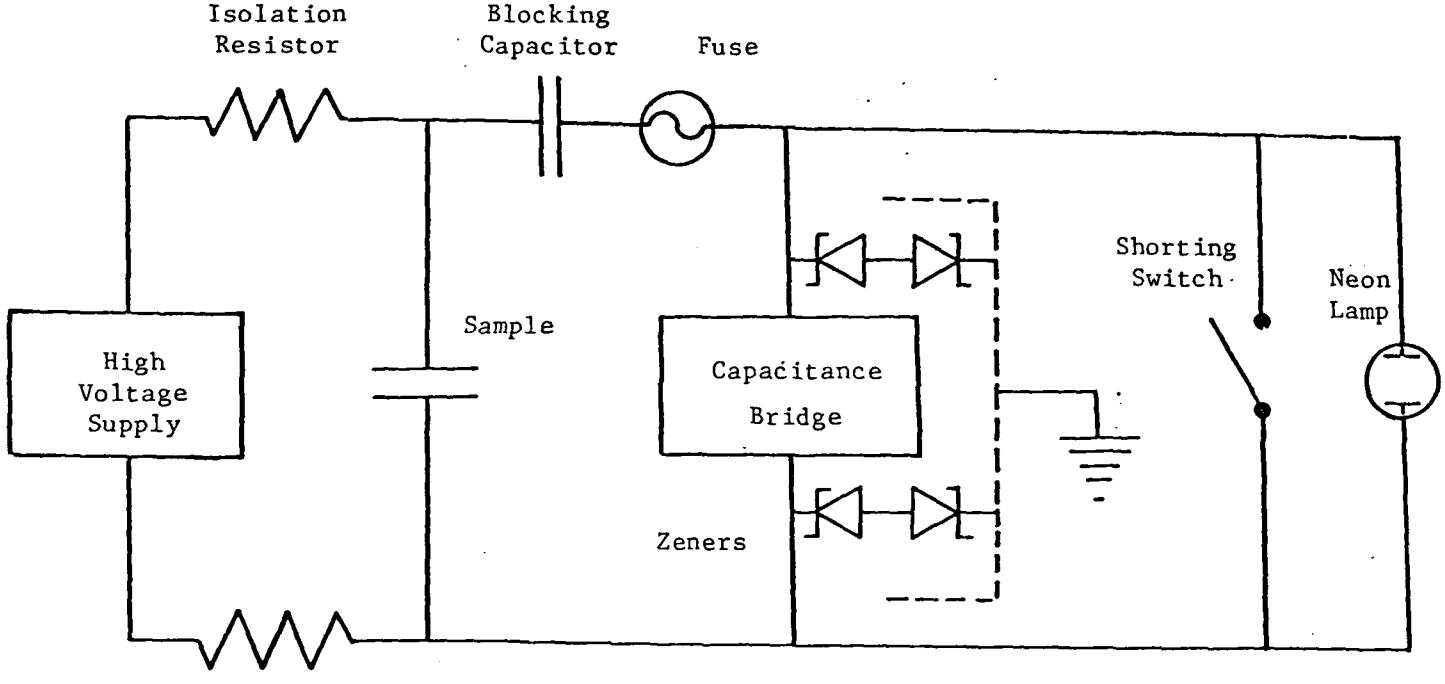

Figure 1. Schematic of the bridge-protection circuitry.

We remark at this point that the fabrication methods used above cannot be optimal and in this short Phase I program there were neither the time nor resources to optimize these fabrication variables.

However, a limited attempt was made to improve the dielectric breakdown strength by making a small, second batch of MLC's starting with much finer reacted powders of CPN17 to improve the homogeneity of the ceramic slurry used in tape casting. The above processing methods were used, and these second-batch MLC's had thinner fired dielectric thicknesses, 28 μm (0.0010 in.). As we shall see, one of these latter MLC's yielded remarkable experimental results.

Dielectric Measurements

According to Eq. (5), the ε_E measurements are central to this study, and for these measurements a General Radio 1620-A Capacitance Measuring Assembly was used. The above design of the MLC's resulted in a very large capacitance value at 77 K, = 4.3 μF, which was beyond the range of the General Radio Bridge, ≤ 1 μF. Consequently, a range-extension capacitor (G.R. 1615-P1) was purchased.

The stored energy density depends on measuring ε_E to large E-fields [i.e., E_c in Eq. (5)], but the insertion unit on the above bridge only protected the detector up to 500 V. Consequently, a bridge-portection circuit was built to extend the applied voltage range to 3000 V, the limit of the Keithley Model 247 Power Supply. A schematic of this circuit is shown in Fig. 1, and the theory of operation is as follows:

When a capacitance measurement of the sample is to be made, the shorting switch is closed, the voltage supply is turned on, and a

The test MLC's were fabricated by standard capacitor-manufacturing methods, as follows. The appropriate starting chemicals were mixed by wet-milling, and, after drying, the powders were calcined at 900°C for 4 hrs. to form reacted CPN17. The ceramic was then ground to a fine particle size (~ 2 μm), mixed with an organic binder, and cast into a "tape" about 80 μm thick. Sections of this tape, approx. 5 x 5 cm^2, were stacked one on top of another with an electrode pattern silk-screened on each section. The electrode paste contained 40% Pt, 40% Au, and 20% Pd, and three cover sheets were left on the bottom and top of the stack.

The stack was next taken through a slow binder-burnout step at 400°C for 24 hr. to remove the organic binders in the tape sections and electrode paste. Finally, the stack was sintered at 1225°C for 1 hr., and in this step the reacted CPN17 powders sinter and fuse together to form a dense, monolithic plate. The individual MLC's are then cut from the plate with a diamond saw.

Twelve MLC's of CPN17 were fabricated in this fashion, and the design parameters were satisfied very well. The MLC dimensions achieved were 0.99 x 0.99 x 0.20 cm^3, and the dielectric thicknesses were 45 μm (.0018 in.).

The densities of these MLC's were somewhat smaller (6.2 - 6.4) than the theoretical density of CPN17 (6.5 gm/cm^3), and so it was decided to hot-isostatically-press half of the MLC's to see if the density could be improved. Unfortunately, a sheer stress developed during this HIP process which delaminated the six MLC's, thus leaving only six MLC's for testing.

voltages, so a 3 μF capacitor from Maxwell Laboratories was measured on the system up to 3 kV, but there no anomalies in the capacitance data. We conclude, therefore, that the data in Fig. 6 are real and are most likely due to field-induced state-switching in CPN17 to a highly polarizable state.

The dielectric breakdown strengths of these prototype MLC's were erratic and smaller than expected. The average breakdown strength of the second batch (~ 260 kV/cm) was improved over the first batch (~ 150 kV/cm), and it is significant that one MLC from each batch withstood 3 kV at 77 K (675 and 1080 kV/cm for these first- and second-batch MLC's, respectively; these values are not included in the averages). Clearly, there were insufficient MLC's for a statistical sampling, but the results suggest that very large breakdown strengths are certainly feasible at cryogenic temperatures in ceramic capacitors.

The data in Figs. 5 and 6 now allow energy-storage estimates according to Eq. (5), and two approaches were taken: (1) The ε_E in Fig. 5 can be numerically integrated up to 200 kV/cm, above which ε_E = 195; and (2) The two upper curves in Fig. 6 can be numerically integrated to point C (1080 kV/cm). The results of these estimates are given in Table I.

Table I

Energy Storage Estimates, Eq. (5)

CPN17 MLC's at 77 K

E_c, kV/cm	ΔF, J/cm^3	ΔF, J/g
214[a]	0.81	0.13
400[b]	1.8	0.28
600[b]	3.4	0.55
900[b]	7.2	1.2
1080[b]	10.5	1.7
1080[c] (induced state)	51-58	8.2-9.4

(a) Limit of Fig. 5 data

(b) Extension of Fig. 5 data

(c) Limit of Fig. 6 data

A CPN17 density of 6.2 g/cm^3 was used to convert ΔF to a gravimetric basis in Table I, and the spread in ΔF-values for the induced-state in Table I reflects the spread in the εE-curves in Fig. 6.

If the highly-polarizable induced state of CPN17 can be stabilized, the Table I estimates show that the ΔF-values associated with this state are quite huge.

VI. SPECIFIC HEAT AND ELECTROCALORIC RESULTS

The zero-field specific heat data for the CPN17 ceramic material in two MLC's (first batch) are shown in Fig. 7 in the range 77 - 110 K.

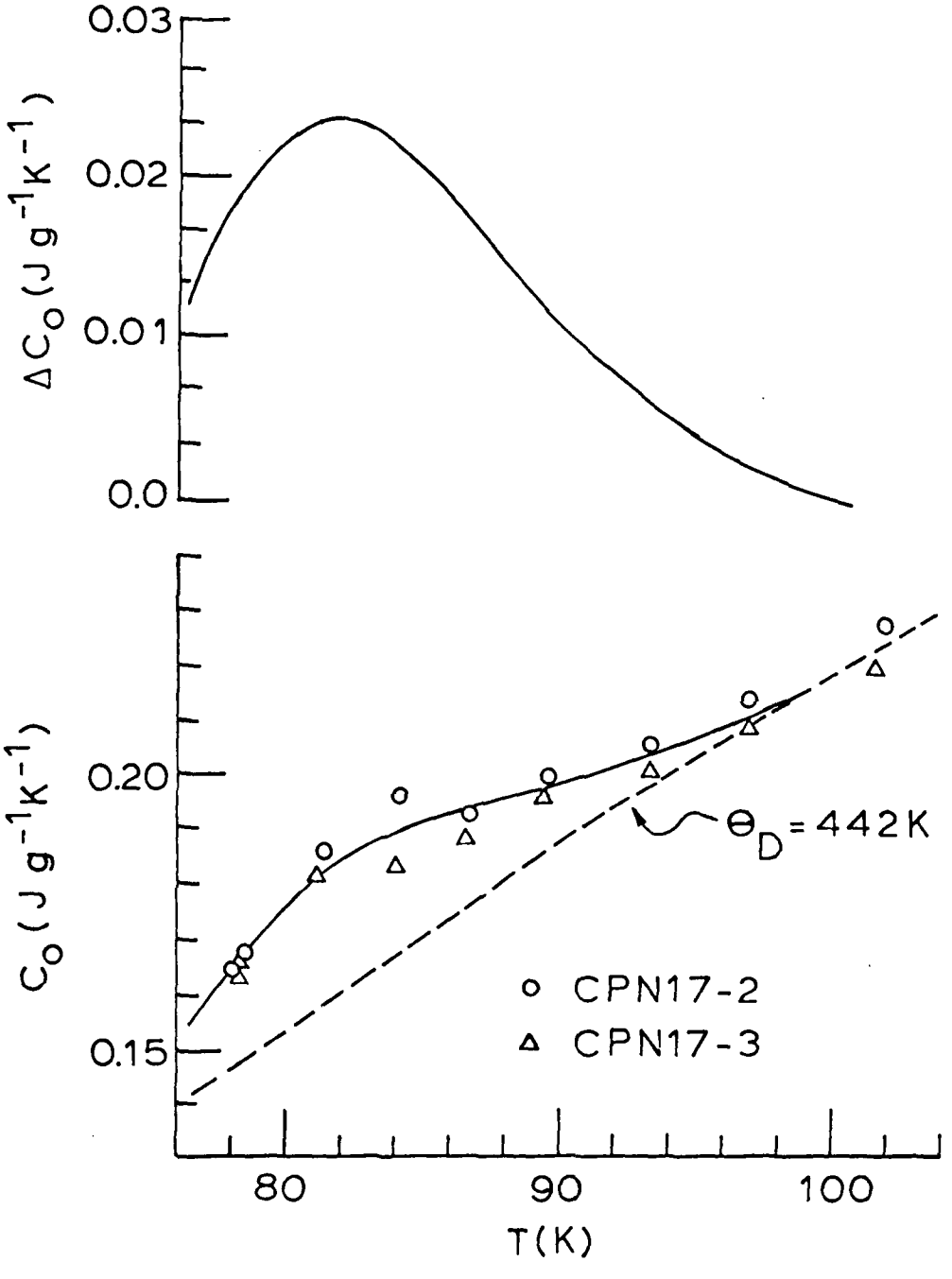

Figure 7. Zero-field specific heat of the CPN17 ceramic material in two MLC's (first batch). An excess specific heat is indicated, upper curve, found by substracting a Debye background specific heat (dashed curve).

The C_0-data for the two MLC's agree quite well, and this serves as a valuable check on the methodology.

The knee in the data at ~ 82 K suggests an excess specific heat associated with the paraelectric-ferroelectric transition. The Fig. 7 data were fitted to a Debye specific heat at the higher temperatures (Θ_D = 442 K) shown by the dashed curve in Fig. 7, and this Debye background was substracted from C_0 to determine the "excess specific heat" ΔC_0-curve in the upper plot. We shall return to this excess specific heat below.

The electric-field dependence of the specific heat of the CPN17 ceramic in several MLC's from both batches is shown in Fig. 8, plotted as C_E/C_0 at several temperatures. An apparently universal, temperature-independent E-field dependence is found, although the effect of a field is relatively small (~ 6% at 200 kV/cm) and appears to saturate at about 200 kV/cm, approximately the same region where ε_E saturates, Fig. 5. Going further, we note from Fig. 7 that the excess specific heat $\Delta C_0 \leq$ 0.02 J g^{-1} K^{-1} compared to the total specific heat ≈ 0.19 J g^{-1} K^{-1}, a 10% effect. Presumably then, the excess specific heat in Fig. 7 represents the E-field-controllable specific-heat component (note that the excess specific heat plot in Fig. 7 depends strongly on the choice of Θ_D).

Electrocaloric temperature-change measurements were made at 77.7 and 94.3 K (average temperatures) on MLC's from the first batch, and it was readily established that the temperature rises (0 → E) and drops (E → 0) were perfectly symmetric; i.e., there was no evidence of hysteretic components. This finding correlates very well with the dielectric ε_E

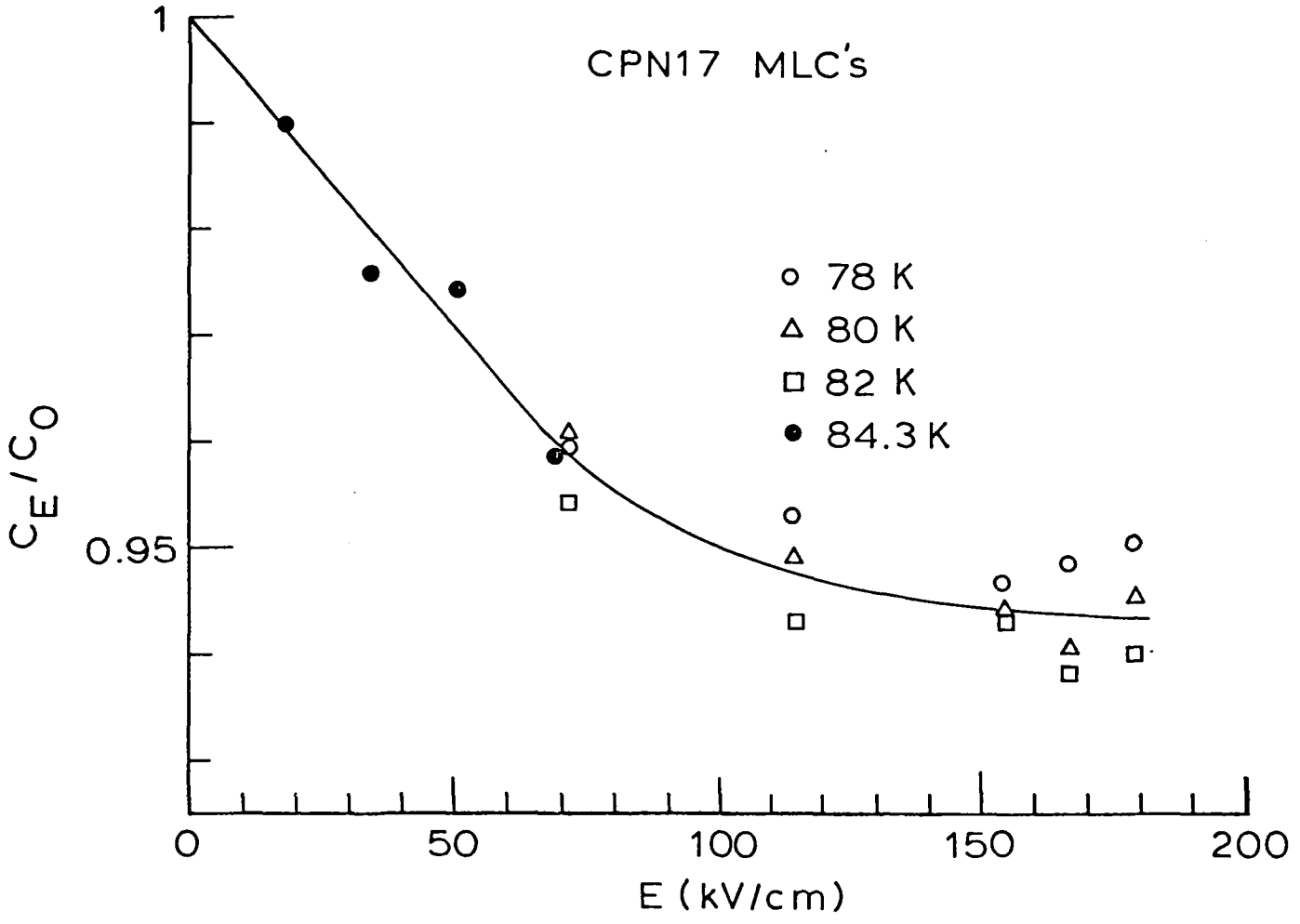

Figure 8. Electric-field dependence of the specific heat of the CPN17 ceramic in several MLC's at the temperatures shown. The solid circles are for MLC's from the first batch, the remaining points, from the second batch. A universal, temperature-independent behavior is suggested.

data in Fig. 4 (note that the dielectric data are measured at 1 kHz, the electrocaloric data at essentially d.c. conditions). These reversible ΔT_e data are shown in Fig. 9 and we point out that in reducing these data according to Eq. (18), the E-field dependence of C_s in Eq. (18) was taken into account using the data in Fig. 8. Referring to Eq. (9), the E^2 leading term is apparent in Fig. 9, and at the highest E-fields an E^6 (or higher-order term) becomes apparent. We note in Fig. 9 that the ΔT_e-values at 77.7 K are <u>smaller</u> than at 94.3 K despite the fact that the specific heat values are ordered oppositely. The thermodynamic analyses in the next section will explain this apparent contradiction.

VII. THERMODYNAMIC ANALYSIS

In this section an attempt will be made to analyze the experimental data in Figs. 3, 5, 7, 8, and 9 along the lines of the theoretical discussion in Section III. The experimental data from the first batch of MLC's are selected because these data represent a complete set.

The first step is to analyze the Fig. 5 data according to Eq. (3) written as

$$4\pi/\varepsilon_E = 4\pi/\varepsilon_0 + \sum b_n E^{2n}. \tag{19}$$

Regression-analysis methods were employed, and it was found that a fourth-order fit (i.e, E^8) gave an excellent representation of the

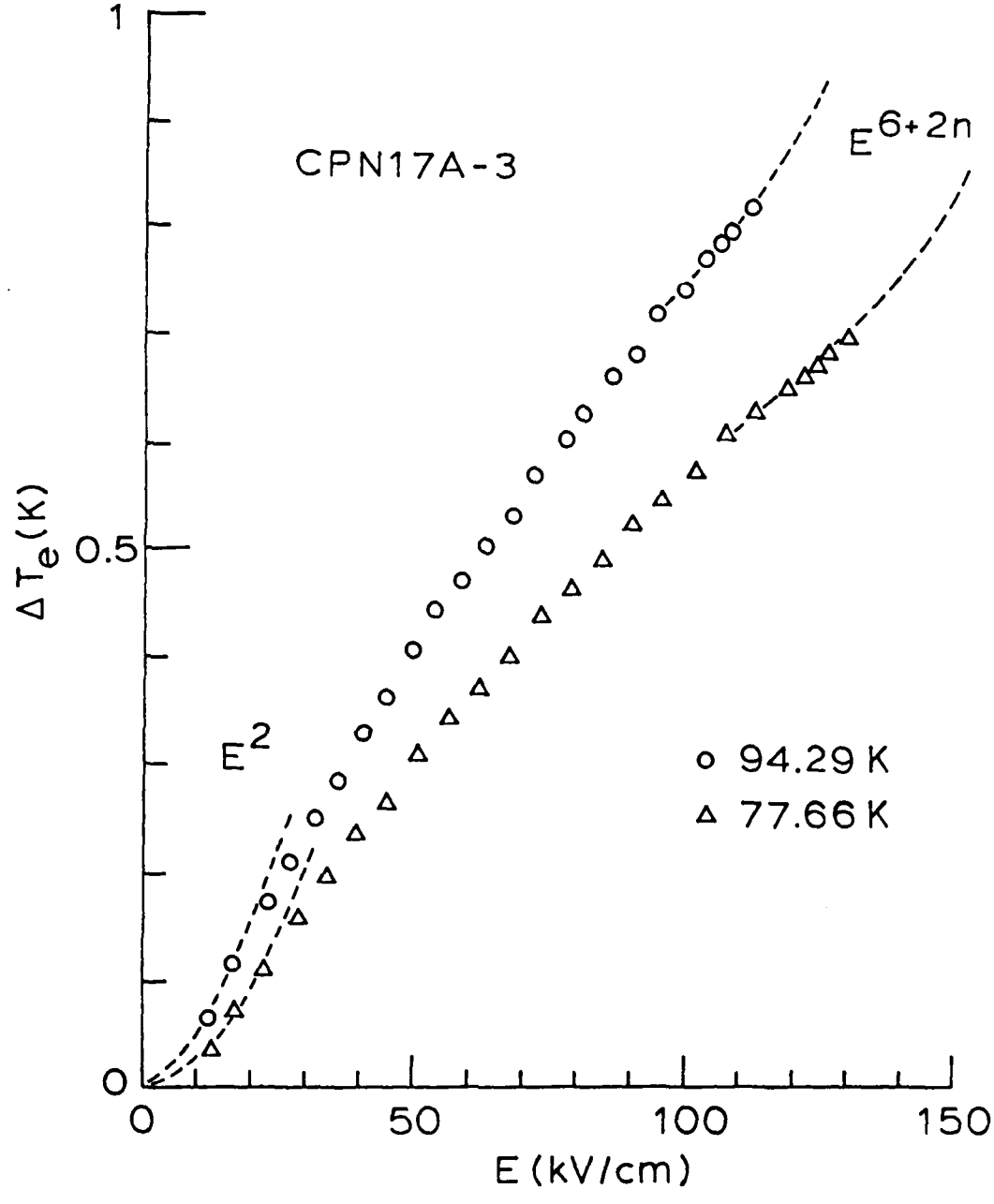

Figure 9. Electrocaloric data measured on CPN17A-3 from the first generation of MLC's at 77.7 and 94.3 K. At low field strengths on E^2 dependence is indicated, changing to an E^6 (or higher order) dependence at the largest fields.

Fig. 5 data. The fitting parameters are given in Table II and are cast in the cgs-esu system of units to facilitate the thermodynamic comparisons below.

Table II

ε_F Fitting Parameters at 77 K[a]

Parameter	Value, cgs-esu
b_1	4.302×10^{-7}
b_2	-2.097×10^{-12}
b_3	5.253×10^{-18}
b_4	-4.767×10^{-24}

(a) Fig. 5 data according to Eq. (19).

Next, the reversible ΔT_e data in Fig. 9 were fitted to Eq. (9) written as

$$\Delta T_e/E^2 = a_0 + a_1E^2 + a_2E^4 + \ldots \tag{20}$$

The experimental data could be fit very satisfactorily with a fourth-order expansion (i.e., E^8) using regression-analysis methods, and these fitting parameters are given in Table III, again in cgs-esu units, for the two temperatures involved.

Table III
ΔT_e Fitting Parameters [a] (cgs-esu)

Parameter	77.7 K	94.3 K
a_0	2.513×10^{-5}	4.325×10^{-5}
a_1	-7.643×10^{-10}	1.997×10^{-9}
a_2	1.133×10^{-14}	4.297×10^{-14}
a_3	-7.204×10^{-20}	3.887×10^{-19}
α_4	1.614×10^{-25}	1.226×10^{-24}

[a] Fig. 9 data according to Eq. (20)

These curve-fittings of the ϵ_E and ΔT_e data involve higher-order terms than appear in Eqs. (3) and (9) to obtain satisfactory data fits, and there is the concern if these two fits are compatible (i.e., E^8 for ϵ_E, E^{10} for ΔT_e). These fits are equivalent for the following reason: The susceptibility χ_E involves the second derivative, Eq. (3), whereas the polarization P involves the first derivative, Eq. (2) (i.e., on inversion). The ΔT_e in Eqs. (8) - (9) involves an integration over E, so an E^m expansion for χ_E is equivalent to an E^{m+2} expansion for ΔT_e.

Comparing Eqs. (9), (10), and (20), we have

$$\dot{x}o/2x_o^2 = (\rho C_o/T)\, a_o \qquad (21)$$

where we have approximated $C_E \simeq C_o$ in Eq. (9) based on the Fig. 8 data and the density ρ enters Eq. (21) because C_E in Eq. (7) is the

volumetric specific heat whereas the Fig. 7 data are gravimetric data. At 77.7 and 94.3 K the a_0-parameters are given in Table III, the χ_0 (= $4\pi/\varepsilon_0$) and C_0 values are taken from Figs. 5 and 7, respectively, and ρ = 6.2 g/cm^3. Solving Eq. (21) we find that $d\varepsilon_0/dT$ = - 82 and - 150 K^{-1} at 77.7 and 94.3, respectively. For comparison, from Fig. 5 we find - 50 and - 110 K^{-1}, respectively, at the two temperatures. This is reasonably good agreement considering the assumptions and approximations used [e.g., using C_0 in Eq. (9) has the effect of overestimating $d\varepsilon_0/dT$ from Eq. (21)].

Again comparing Eqs. (9), (10), and (20) as above, we have

$$-\xi \dot{\chi}_0/\chi_0^5 = (\rho C_0/T)a_1, \tag{22}$$

and proceeding as above and using experimental data for $d\varepsilon_0/dT$, we find that

$$\xi(77.7\ \text{K}) = 2.69 \times 10^{-13}\ \text{(cgs-esu)}$$
$$\xi(94.3\ \text{K}) = 3.63 \times 10^{-1}\ \text{(cgs-esu)}. \tag{23}$$

Turning now to the ε_E-data, we have on comparing Eqs. (3) and (19) that

$$3\xi/\chi_0^2 = b_1 \tag{24}$$

which from Table II and Fig. 5 yields

$$\xi(77.4\ \text{K}) = 4.31 \times 10^{-13}\ \text{(cgs-esu)} \tag{25}$$

The agreement between the ξ-values from the electrocaloric data, Eq. (23), and the dielectric data, Eq. (25), is very satisfying considering the amount of experimental data used and the assumptions made. Summarizing,

$$\xi = (3.54 \pm 0.81) \times 10^{-13}\ \text{(cgs-esu)}. \tag{26}$$

Turning next to the ς-coefficient, we have on comparing Eqs. (9), (10), and (20) that

$$21\xi^2\dot{\chi}_o/6\chi_o^8 - \xi\dot{\chi}_o/\chi_o^7 = (\rho C_o/T)a_2, \tag{27}$$

which yields from the electrocaloric data

$$\begin{aligned}\varsigma(77.7\ \text{K}) &= 2.48 \times 10^{-22}\ \text{(cgs-esu)}\\ \varsigma(94.3\ \text{K}) &= 1.64 \times 10^{-22}\ \text{(cgs-esu)}\end{aligned} \tag{28}$$

using the average ξ-value from Eq. (26). For the dielectric data, on comparing Eqs. (3) and (19),

$$5\varsigma/\chi_o^4 - 6\xi^2/\chi_o^5 = b_2, \tag{29}$$

which yields on substitution of the appropriate quantities

$$\varsigma(77.4\ \text{K}) = 0.86 \times 10^{-22}\ \text{(cgs-esu)} \tag{30}$$

Once again there is a satisfying agreement between the electrocaloric and dielectric data, and the average value of ζ is

$$\zeta = (1.66 \pm 0.81) \times 10^{-22} \text{ (cgs-esu)} \tag{31}$$

Therefore, we find that the dielectric data (Figs. 3 and 5), specific-heat data (Fig. 7), and electrocaloric data (Fig. 9) can be satisfactorily explained and correlated along the thermodynamic lines given in Section III. Only the χ_0-coefficient was assigned a temperature dependence, and the E-field dependence of the specific heat was ignored, yet we find remarkably good agreement between the ξ and ζ coefficients determined independently. The sign of the ξ-coefficient indicates that the ferroelectric transition in CPN17 is second order.

Finally, it is of interest to compare the ξ and ζ coefficients here with those for other ferroelectrics, and this comparison is given in Table IV.

Table IV

Comparison of Ginzburg-Landau Coefficients (cgs)

	CPN17	$KTaO_3$ (a)	$SrTiO_3$ (b)	$BaTiO_3$ (c)
ξ	3.54×10^{-13}	9.8×10^{-12}	$\sim 10^{-12}$	$\sim 1.2 \times 20^{-12}$
ζ	1.66×10^{-22}	6.2×10^{-20}	3×10^{-21}	$\sim 5 \times 10^{-22}$

(a) Ref. 10

(b) Ref. 11

(c) Ref. 12

VIII. CONCLUSIONS AND DISCUSSION

The technical goals of this Phase I program have been met in that: (1) Prototype, multilayer capacitors were successfully fabricated; (2) Dielectric, specific-heat, and electrocaloric data were measured on these MLC's and successfully explained within the Ginzburg-Landau thermodynamic formalism; and (3) Capacitive energy storage values at 77 K in the range 1 - 10 J/g were determined from measured εE-data.

The state-switching phenomenon in Fig. 6 is of great interest both from a practical viewpoint and also from a fundamental viewpoint. Clearly, if this state can be stabilized, the energy storage density (~ 10 J/g) associated with this state is very large, approaching the density of chemical explosive systems.

The explanation of the ε-E behavior in Fig. 6 is probably straightforward: For E ≈ 300 kV/cm, CPN17 undergoes a field-induced phase transition to a highly polarizable state. The CPN17 material is a pyrochlore structure, space group Fd3m, and this structure is especially favorable for induced phase transitions. That is, there are eight $A_2B_2O_7$ units per unit cell, so there are multiple, possible, neighboring states involving, for example, slight rotations of oxygen octahedra. For comparison, the perovskite structure (point group m3m) contains one formula weight per unit cell, so that phase transitions involve rather gross distortions (e.g., cubic → tetragonal) and the number of neighboring states is small (3). One imagines that in the $A_2B_2O_7$ pyrochlore structure, the dielectric activity is dominated by the displacement of B-site ions within the BO_6 octahedra. On increasing E, these displacements begin to saturate along the field direction, but at a certain

E-field the BO_6 octahedra may rotate, thus providing unsaturated directions for B-site ion displacement, and therby a sharp jump in ε_E as in Fig. 6.

It is particularly important that ε_0 repeats very well, Fig. 6, as this indicates that the induced state in CPN17 is <u>non-hysteretic</u> which is very important for capacitive energy storage. That is, if this induced state had a spontaneous polarization, ε_0 would be considerably reduced as $E \to 0$. The repeatability of ε_0 simply means that all the accessible states of the B-site ion at $E = 0$ are still available after field-cycling to $\sim$ 1 MV/cm.

The dielectric breakdown strengths achieved in the prototype MLC's were somewhat disappointing, but this is not surprising considering these were the first attempts to make CPN17 MLC's. Nonetheless, it is significant that the average breakdown strengths were improved between the first and second (small) batches of MLC's and that one MLC withstood 1.07 MV/cm.

The success of the thermodynamic analysis in explaining and correlating all the data measured on the first-batch MLC's is very satisfying and explains why the ΔT_e's at 94.3 K are <u>larger</u> than at 77.7 K in Fig. 9. Namely, $d\varepsilon_0/dT$ is <u>larger</u> at the former temperature. Since the transition temperature and therefore $d\varepsilon_0/dT$ can be changed by varying the composition of the CPN17 ceramic, this finding is of great practical interest for adjusting the electrocaloric effects.

The electrocaloric effects may act as a stabilizing mechanism in certain fast-discharge applications, and the electrocaloric energy available can be estimated directly from the specific heat data in Fig. 7: At 77 K, the CPN17 ceramic has $C_0 \simeq 0.15$ J g^{-1} K^{-1}, so for an

adiabatic-depolarization temperature change ~ 1 K (Fig. 9) the energy available is ~ 0.15 J g^{-1} = 0.93 J cm^{-3}.

These electrocaloric effects must be viewed in the correct light: On polarization, a heating effect takes place, whereas on depolarization, a cooling effect occurs, and these two effects are equal because the electrocaloric effects are reversible. Consequently, the electrocaloric properties do not affect the overall system energy balance at steady state.

However, this does not mean that electrocaloric effects are without value. For example, one can imagine a slow charging situation where the heat of polarization diffuses into the nitrogen bath followed by a fast discharge where electrocaloric cooling compensates for the slow diffusion of irreversible heating effects (see below). Thus, while not affecting the energy balance, electrocaloric effects could favorably impact the rate of charge/discharge cycling.

Finally, we return to the Joule heating in the thin metal electrodes in the MLC, Eq. (15),

$$U \simeq (\rho_e/\delta)(\omega \ell^3)\Delta t)(\Delta F/E_c)^2$$

where from Section IV ρ_e/δ = 3.14 Ω at 77 K. Selecting the realistic values $\ell = \omega$ = 2.54 cm and $\Delta t = 10^{-2}$ sec, and taking the most extreme case from the above data, ΔF = 9.4 J/g = 58 J/cm^3 (Table I) at E_c = 1.08 MV/cm, we find

$$U \simeq 4 \times 10^{-5} \text{ J}.$$

This Joule heating is absorbed by the ceramic layer, and selecting d = 0.001 in. we find that the energy density to be absorbed by the ceramic layer is 2.44×10^{-3} J/cm^3. Since the specific heat of the CPN17 at 77 K is 0.15 J g^{-1} K^{-1} = 0.93 J cm^{-3} K^{-1}, the associated temperature rise in the ceramic is ~ 2 1/2 mK. This is a very small temperature rise compared to the electrocaloric temperature changes. In fact, since $U \propto (\Delta t)^{-1}$, the discharge time would have to approach ~ 25 μsec before the Joule heating in the electrode would become equivalent to the electrocaloric cooling for this extreme case.

IX. RECOMMENDATIONS FOR FUTURE STUDIES - PHASE II

The studies here indicate three related areas for research in a Phase II study: (1) Ceramic research to understand and thereby improve the breakdown strength of CPN17 MLC's at cryogenic temperatures; (2) Solid-state research to understand the physics of CPN17 at large electric fields in general and of the state-switching phenomenon in particular, including the development of thermodynamic models; and (3) Systems research based on the construction and testing of a prototype capacitive-energy-storage system, including a thermodynamic systems analysis. We note that the studies (2) and (3) above depend on the first study.

A Phase II program along these lines would not only yield fundamental ceramic and solid-state physics information but also generate operating data for a prototype storage system.

REFERENCES

[1] K.N. Mathes and S.H. Minnich, Cryogenic Capacitor Investigation, General Electrical Co., Final Report S-67-1095, May, 1965.

[2] W.N. Lawless, Proc. XIII Int'l Congress of Refrigeration, Washington, D.C., 1971, Vol. 1, p. 599.

[3] A.F. Devonshire, Adv. in Physics 3, 85 (1954).

[4] W.R. Buessem, L.E. Cross, and A.K. Goswami, J. Amer. Ceram. Soc. 49(1), 33 (1966).

[5] W.N. Lawless, J. Phys. Chem. Solids 30, 1161 (1969).

[6] W.N. Lawless, Phys. Rev. B14, 134 (1976).

[7] W.N. Lawless, Rev. Sci. Instrum. 48, 361 (1977).

[8] R.J. Corruccini and J.J. Gniewek, NBS Monograph 21, Oct. 1960.

[9] J.T. Heesels, Cryogenics 11, 483 (1971) and references therein.

[10] W.N. Lawless, Phys. Rev. B16, 433 (1977).

[11] W.N. Lawless and A.J. Morrow, Ferroelectrics 15, 159 (1977).

[12] F. Jona and G. Shirane, Ferroelectric crystals (Pergamon Press, New York, 1962).

END

FILMED

7-85

DTIC